NJC

New Journal of Chemistry

A journal for new directions in chemistry

Accepted Manuscript

This article can be cited before page numbers have been issued, to do this please use: Ø. Gullbrekken and S. K. Schnell, *New J. Chem.*, 2023, DOI: 10.1039/D3NJ04065H.

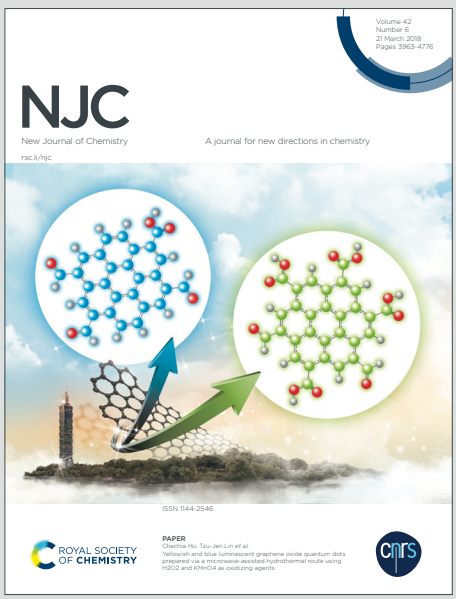

This is an Accepted Manuscript, which has been through the Royal Society of Chemistry peer review process and has been accepted for publication.

Accepted Manuscripts are published online shortly after acceptance, before technical editing, formatting and proof reading. Using this free service, authors can make their results available to the community, in citable form, before we publish the edited article. We will replace this Accepted Manuscript with the edited and formatted Advance Article as soon as it is available.

You can find more information about Accepted Manuscripts in the Information for Authors.

Please note that technical editing may introduce minor changes to the text and/or graphics, which may alter content. The journal's standard Terms & Conditions and the Ethical guidelines still apply. In no event shall the Royal Society of Chemistry be held responsible for any errors or omissions in this Accepted Manuscript or any consequences arising from the use of any information it contains.

View Article Online
DOI: 10.1039/D3NJ04065H

Journal Name

ARTICLE TYPE

Cite this: DOI: 00.0000/xxxxxxxxxx

Coupled Ion Transport in Concentrated PEO-LiTFSI Polymer Electrolytes†

Øystein Gullbrekken, Sondre Kvalvåg Schnell*

Received Date
Accepted Date

DOI: 00.0000/xxxxxxxxxx

Understanding how microscopic mechanisms govern macroscopic transport properties is important for development of improved electrolytes for Li-ion batteries. The archetypal polymer electrolyte PEO-LiTFSI has been investigated for more than three decades, but the fundamental ion transport mechanisms are still elusive. Molecular Dynamics (MD) simulations enable us to determine transport properties by directly probing particle movements. Both transport properties and microscopic interactions that govern them can be studied simultaneously. In this work, ionic conductivity and transport numbers of PEO-LiTFSI electrolytes are computed as a function of salt concentration and PEO chain length. The values are obtained using the Nernst-Einstein approximation for dilute or ideal systems, in addition we determine the Onsager coefficients that take into account ionic correlations. We observe significant differences between the two methods, indicating non-ideality. The motion of Li and TFSI is anticorrelated, causing super-ionicity. We discuss the relevance of the frame of reference. The static and dynamic properties of Li-ion coordination environments are analyzed. The distributions of cation-solvent and cation-anion residence times are investigated and indicate that the TFSI facilitate Li transport and Li jumps in the polymer network. Finally, the thermodynamic factors are computed and used to quantify the non-ideality of the systems.

1 Introduction

Polymer electrolytes was initially introduced by Wright *et al.*[1,2] in the 1970s, where it was shown that poly(ethylene oxide) (PEO) had the ability of dissolving- and conducting alkali metal ions at close to ambient temperature. The metal cations are coordinated by units of Lewis base in the polymer, specifically by ether oxygen atoms in PEO[3]. Armand analyzed the properties of the new class of materials for electrochemical purposes in 1983[4], and suggested *lithium bis(trifluoromethanesulfonyl)imide* (LiTFSI) as a salt together with PEO[5] for use in Li-ion batteries. PEO-LiTFSI has since been widely investigated as a polymer electrolyte[6]. Li is typically coordinated by 5 to 6 ether oxygen atoms in PEO[7], and the TFSI-anion is known for its plasticizing effect, arising due to the flexibility of the $-SO_2-N-SO_2-$ segment, which reduces the crystallinity of the PEO and thus increases the ionic conductivity. Additionally, LiTFSI dissociates easily due to the large size and low charge density of the anion[3]. However, the ionic conductivity of PEO-LiTFSI electrolytes is too low at room temperature for commercial applications, about $10^{-6}\,\mathrm{S\,cm^{-1}}$ and the Li-ion transport number is found to be low in many studies, about 0.2 or lower[3,6,8–10].

Li-ion transport in PEO-based electrolytes occurs by three main mechanisms: The Li-ions can jump from ether oxygen to ether oxygen along a PEO chain, called *intrachain* transport, or they can jump between PEO chains, called *interchain* transport[11]. Both of these transport mechanisms occur by changing coordination environment and are called structural diffusion[12]. Vehicular diffusion with the PEO chains, without changing coordination, is the third transportation mode of Li-ions. Consequently, the mobility of Li-ions is closely coupled to the motion of the polymer backbone and occurs in the amorphous phase where the polymer chains can move freely[3].

Molecular Dynamics (MD) simulations is a powerful tool to investigate transport properties in electrolytes and have been used in various studies[11,13–22]. Average charge transport properties, such as ionic conductivity and transport numbers, can be determined by studying equilibrium fluctuations in simulations[21,23]. Simultaneously, it is possible to analyze the molecular and ionic correlations that govern the average properties. The distribution of values beneath the averages can be exposed and examined as the trajectory of every particle is known. This combination is useful for a more complete understanding of the transport properties in electrolytes. It is common to utilize the Nernst-Einstein (NE)

Department of Materials Science and Engineering, Norwegian University of Science and Technology, NTNU, NO-7491 Trondheim, Norway. E-mail: sondre.k.schnell@ntnu.no.

† Electronic Supplementary Information (ESI) available: Finite size effects, coordination data, experimental ionic conductivity, Onsager coefficients involving solvent, Maxwell-Stefan coefficients, radial distribution functions, distribution of pair lifetime correlations at selected time intervals, and calculation of anion coordination of different parts of the distributions. See DOI: 00.0000/00000000. LAMMPS inputfiles, and relevant scripts can be found at: DOI: 10.5281/zenodo.10000803

View Article Online
DOI: 10.1039/D3NJ04065H

approximation, based on the self-diffusion coefficients, when analyzing the charge transport properties[14–17,21,24]. Nernst-Einstein is an approximation for dilute or ideal systems, where ionic correlations are neglected. Here, we analyze the transport properties both in terms of the self-diffusion coefficients and NE approximation, as well as in terms of the Onsager coefficients which takes ionic and molecular correlations into account.

In this work, we aim to understand the macroscopic ionic transport properties of PEO-LiTFSI polymer electrolytes from microscopic interactions. We show how to compute the ionic conductivity and transport numbers from equilibrium MD simulations using the NE approximation and the Onsager coefficients in the Theory section. The differences of the two methods are emphasized. The ionic conductivity and transport numbers of the PEO-LiTFSI systems computed with the NE approximation and Onsager coefficients are presented in the Results section. We observe significant differences between the two methods and discuss these. We discuss the significance of reference frame when analyzing and comparing transport numbers and transport coefficients. The static and dynamic properties of the Li coordination environments are characterized to understand the microscopic transport mechanisms of Li. Finally, we present the computed thermodynamic factor of the PEO-LiTFSI systems and relate it to the above findings.

2 Theory

Diffusion is potentially the limiting factor in transport of mass and charge in polymer electrolytes[25]. Transport and diffusion properties in electrolytes can be studied in equilibrium MD simulations by sampling the equilibrium fluctuations of particle displacements or velocities, or using the Einstein or Green-Kubo relations, respectively[21]. Both methods are in principle equivalent[13]. We used the Einstein relations to study the transport properties in this work, as plots of the mean squared displacement can indicate how well the system has converged[26].

The Nernst-Einstein approximation or the Onsager coefficients can be used to examine the charge transport properties of electrolytes. The NE approximation is based on the Nernst-Einstein equation which relates the diffusion coefficient directly to the mobility of a species[13]. Hence, it is well suited for dilute and ideal systems. In MD simulations, the NE approximation is based on the self-diffusion coefficients[14–17,21,24], which is calculated from the mean squared displacement or velocities of particles. The self-diffusion coefficients are defined when there is no chemical potential gradient influencing the transport, *i.e.* they describe the movements of individual particles in the absence of a field. The self-diffusion coefficient of component i is:

$$D_{i,\mathrm{self}} = \lim_{t\to\infty} \frac{1}{6N_i} \frac{\mathrm{d}}{\mathrm{d}t} \left\langle \sum_{k=1}^{N_i} \left(\mathbf{r}_{k,i}(t) - \mathbf{r}_{k,i}(0)\right)^2 \right\rangle, \tag{1}$$

where t is time, $\mathbf{r}$ is the particle position vector, N_i is the number of particles of component i and the $\langle\cdots\rangle$ brackets denote an ensemble average. The resulting NE approximation of the partial ionic conductivity contribution by species i is:

$$\sigma_i^{\mathrm{NE}} = \frac{z_i e N_i D_{i,\mathrm{self}}}{k_{\mathrm{B}} T V}, \tag{2}$$

where k_{B} is the Boltzmann constant, T is absolute temperature, V is system volume, z_i is the charge valency of species i, and e is the elementary charge. The NE total ionic conductivity is obtained by summing all partial ionic conductivity contributions: $\sigma^{\mathrm{NE}} = \sum_i \sigma_i^{\mathrm{NE}}$. The NE transport number of species i is:

$$t_i^{\mathrm{NE}} = \frac{\sigma_i^{\mathrm{NE}}}{\sum_i \sigma_i^{\mathrm{NE}}} = \frac{\sigma_i^{\mathrm{NE}}}{\sigma^{\mathrm{NE}}}. \tag{3}$$

To study the transport properties of concentrated electrolytes, we need to include deviations from the NE approximation by evaluating the contributions from molecular and ionic correlations. These are included in the Onsager coefficients:

$$L_{ij} = \frac{1}{6N} \lim_{t\to\infty} \frac{\mathrm{d}}{\mathrm{d}t} \left\langle \left(\sum_{k=1}^{N_i} \left[\mathbf{r}_{k,i}(t) - \mathbf{r}_{k,i}(0)\right] \right) \left(\sum_{l=1}^{N_j} \left[\mathbf{r}_{l,j}(t) - \mathbf{r}_{l,j}(0)\right] \right) \right\rangle, \tag{4}$$

in which N_i and N_j are the numbers of particles of component i and j, respectively, and N is the total number of particles in the system. Note that i and j might denote the same or different components. L is a general transport coefficient which gives the transport due to a gradient, *e.g.* an electric field or a thermal field. Here, L_{ij} describes the transport of species i in a chemical potential gradient of species j. L_{ii} describes the transport of species i in a chemical potential gradient of species i, which includes the self-diffusion contribution. An electrolyte with n species can be described by $n(n-1)/2$ independent Onsager coefficients according to Onsager's reciprocal relations[27]. Thus, a binary electrolyte composed of a salt in a solvent has three independent Onsager coefficients[27]. The corresponding expression for the ionic conductivity contribution of the correlation between species i and j is[23,28]:

$$\sigma_{ij} = \frac{e^2}{6k_{\mathrm{B}}TV} \lim_{t\to\infty} \frac{\mathrm{d}}{\mathrm{d}t} \left\langle \sum_{k=1}^{N_i} \sum_{l=1}^{N_j} z_i z_j \left[\mathbf{r}_{k,i}(t) - \mathbf{r}_{k,i}(0)\right] \cdot \left[\mathbf{r}_{l,j}(t) - \mathbf{r}_{l,j}(0)\right] \right\rangle. \tag{5}$$

The total ionic conductivity is obtained by summing over all ionic pairs:

$$\sigma = \sum_i \sum_j \sigma_{ij}, \tag{6}$$

and we call this the Onsager ionic conductivity. The Onsager transport number of a species i is:

$$t_i = \frac{\sum_j \sigma_{ij}}{\sigma}, \tag{7}$$

where we sum over all the partial conductivity contributions of species i computed with equation (5) in the numerator[29].

The effect of ionic correlations in an electrolyte can be quantified as the ionicity, also called the inverse Haven's ratio[30]. The ionicity is defined as the Onsager ionic conductivity divided by the Nernst-Einstein ionic conductivity. If ionic correlations decrease the ionic conductivity, the ionicity will be below one.

View Article Online
DOI: 10.1039/D3NJ04065H

Residence time

The average residence time of two species pairs i and j is calculated using the normalized lifetime correlation function, $P_{ij}(t)$[28,31]:

$$P_{ij}(t) = \frac{\langle H_{ij}(t)H_{ij}(0)\rangle}{\langle H_{ij}(0)H_{ij}(0)\rangle}, \tag{8}$$

and $H_{ij}(t)$ which denotes whether the species are together or not:

$$H_{ij}(t) = \begin{cases} 1, & d_{ij}(t) \leq r_c \\ 0, & d_{ij}(t) > r_c \end{cases} \tag{9}$$

where $d_{ij}(t)$ is the distance between species i and j at time t and r_c is the specified cutoff distance. The $\langle \cdots \rangle$ brackets denote an ensemble average. The cutoff distance was chosen as the first minimum after the first peak in the radial distribution function (RDF) of i and j. The actual cutoffs for the different systems are given in Table S6 (ESI†). The lifetime correlation function in equation (8) is computed using the total time that the species pairs i and j are closer than the specified cutoff distance. This means that if the pair separates and later joins back together, $P_{ij}(t)$ will continue to increase. Hence, we are computing the so-called intermittent residence time. The lifetime correlation function was fitted to the following equation[32]:

$$P_{ij}(t) = \sum_i a_i \exp\left(\frac{-t}{b_i}\right), \tag{10}$$

where a_i and b_i are fitting parameters and the number of terms in the summation was adjusted to optimize the fit such that the standard deviation of the parameters was below 6 % of the values. The fitted function was integrated to determine the average residence time of species i and j[32]:

$$\tau_{ij} = \int_0^\infty P_{ij}(t)\mathrm{d}t. \tag{11}$$

Thermodynamic factor

The thermodynamic factor, Γ, is a way of quantifying the ideality of a mixture. In a binary electrolyte, it can be defined as[9,33]:

$$\Gamma = 1 + \frac{\mathrm{d}\ln\gamma_\pm}{\mathrm{d}\ln x}, \tag{12}$$

where $\gamma_\pm$ is the molar activity coefficient of the salt and x is the mole fraction of the salt. For an ideal mixture, $\gamma_\pm = 1$ and $\Gamma = 1$. Negative Γ indicates thermodynamically unstable mixtures of binary systems. Thermodynamic factors can be computed from MD simulations using Kirkwood-Buff integrals (KBI). Kirkwood-Buff theory relates the microscopic structure of isotropic liquids described by RDFs to their thermodynamic properties. We used the pseudo-binary approach to compute KBIs of the electrolyte systems where the anions and cations are treated as similar molecules, *i.e.* one component[34–36]. The ether oxygens were considered as the solvent. For a binary mixture consisting of species i and j, the Kirkwood-Buff integral of a finite spherical volume L is[35]:

$$G_{ij}^V = \int_0^L [g_{ij}(r) - 1]4\pi r^2 \left(1 - \frac{3x}{2} + \frac{x^3}{2}\right)\mathrm{d}r, \tag{13}$$

where r is the radius, $x = r/L$ and the radial distribution functions, g_{ij}, of the pseudo-binary system are obtained from the RDFs of the ternary system[35]. Finally, the thermodynamic factor is computed by[26,37,38]:

$$\Gamma = 1 - \frac{x_i\rho_j(G_{ii} + G_{jj} - 2G_{ij})}{1 + \rho_j x_i(G_{ii} + G_{jj} - 2G_{ij})}, \tag{14}$$

where x_i is the mole fraction of species i and ρ_j is the average number density of species j. In an ideal mixture, the interactions between like and unlike components are equal, the expression $G_{ii} + G_{jj} - 2G_{ij}$ becomes zero and Γ becomes one.

3 Method

The transport properties were characterized by running MD simulations using the LAMMPS[39] software on all-atom PEO-LiTFSI polymer electrolyte systems with varying salt concentrations and PEO chain lengths. We used the OPLS-AA potential[40] to describe intra- and intermolecular interactions. The parameters for PEO were obtained from the Ligpargen web server[41–43], the Li cation parameters from Jensen and Jorgensen[44], and we used the parameters developed by Canongia Lopes and Pádua for the TFSI anion[45]. We used Moltemplate[46] to build longer polymer chains from the templates supplied by Ligpargen. Shorter template chains were joined together to create chains of the desired length. The assigned electric charges of the atoms near the template chain ends will differ from the more central atoms due to different chemical environments. The electric charge of the atoms near the interconnected chain sites were manually adjusted to obtain consistent charges of similar atom types and to achieve overall electroneutrality. The C−H bonds of the polymer were fixed at the equilibrium bond length using the SHAKE algorithm[47] with an accuracy tolerance of 1×10^{-6}. Intramolecular Lennard-Jones and Coulombic forces between nearest and next-nearest neighbors were switched off while interactions between atoms separated by two atoms were halved, as is standard in OPLS[40,41]. Global cutoffs for the Lennard-Jones and Coulombic forces were set to 11 Å. Geometric mixing rules were used to determine the Lennard-Jones interactions between unlike atoms. Long-range Coulombic forces were solved using a particle-particle particle-mesh solver[48] with a relative error in forces of 1×10^{-6}. The ionic charges were scaled by a factor of 0.75 to account for the typical overestimation of Coulombic interactions between ions in non-polarizable force fields[49]. Periodic boundary conditions were applied in all directions. Initial configurations of the most dilute systems were prepared by placing PEO chains, and Li and TFSI ions in a simulation box with the Packmol software[50].

The equilibration and simulation details are described in the following. Firstly, the energy of the simulation box was minimized to avoid particle overlap. Then, the systems were equilibrated to obtain probable local energy minimum structures of the polymer electrolytes. We adopted an equilibration routine composed of a series of annealing and compression/decompression steps, developed by Molinari *et al.*[20] In order for the density and potential energy of the systems to converge, additional equilibration at temperatures of 390 K and 400 K was performed in the isothermal-isobaric (NPT) ensemble with a pressure of 1 atm and a timestep of 1 fs. The final equilibration was done at 423 K and

View Article Online
DOI: 10.1039/D3NJ04065H

1 atm with a timestep of 1.25 fs. The Nosé-Hoover thermostat and barostat[51–53] were used to control the temperature and pressure in the NPT ensemble with time constants resulting in characteristic thermal and pressure fluctuations of 100 and 1000 timesteps, respectively. The lengths of the box sides were relaxed to facilitate the equilibration procedure. When the density and potential energy of the systems were stabilized, we switched to the canonical (NVT) ensemble to conduct production simulation runs. The volume of the simulation box was scaled according to the average volume during the final equilibration at 423 K to obtain correct density in the NVT ensemble. The Nosé-Hoover thermostat with thermal fluctuations of 100 timesteps was used to control the temperature in the NVT ensemble. Production runs lasted for at least 100 ns, which was sufficient to reach the diffusive regime of most diffusion coefficients. It is noted in the text which coefficients are not computed from the diffusive regime. In order to achieve sufficiently fast dynamics and reduced simulation times, we ran simulations at a temperature of 423 K with a timestep of 1.25 fs. Simulating at this temperature should not dramatically influence the trends of the dynamic properties compared to the normal operating temperatures of these electrolytes of around 350 K. The systems with lowest salt concentration were prepared and sampled first. Then, the systems with higher salt concentrations were made consecutively by randomly placing more Li and TFSI to the configuration at the end of the production runs, followed by energy minimization and equilibration. The equilibration following salt addition was conducted by firstly running 5 million time steps of 1 fs at 390 K and 1 atm with a soft potential[54] utilizing a softness parameter of 0.5 to facilitate rapid mixing of polymer chains and ions. Next, the full potential was turned back on for 55 million time steps at 390 K and 1 atm, followed by at least 30 million time steps of 1.25 fs at 400 K and finally at least 20 million time steps of 1.25 fs at 423 K. The average box volume was sampled during the run at 423 K to adjust the box volume to the correct size before the production run in the NVT ensemble. The total energy of every system was sampled in the microcanonical (NVE) ensemble before the production run to check the stability of the systems. The change of total energy in the NVE ensemble was normally below 1 kcal mol^{-1} ns^{-1}, and always below 2 kcal mol^{-1} ns^{-1}, corresponding to less than 1 % change of the total energy during 100 ns. The transport properties were sampled in the NVT ensemble.

The salt concentrations studied corresponded to ethylene oxide (EO):Li ratios of 50, 20, 10, 6, 3 and 2, or equivalently Li:EO ratios of 0.02, 0.05, 0.10, 0.17, 0.33 and 0.50. We investigated the effect of PEO chain length on the ion dynamics. Two PEO chain lengths were investigated, 23 and 100 monomers (EO) long. 172 chains of length 23 monomers or 40 chains of length 100 monomers were placed in the simulation box, giving about 4000 monomers of each. All PEO chains in each simulation box had the same length. The PEO chains were methoxy-/ethoxy-terminated with $-O-CH_3$ termination on one end and $-O-CH_2-CH_3$ on the other. We used the OCTP module[55] to calculate self-diffusivities and Onsager coefficients. The KBIs G_{ij} in the thermodynamic limit were estimated by plotting G^V_{ij} against $1/L$ where L is the radius of the volume and determining the intercept by extrapolating the linear range of the curve[56]. The nitrogen atom and the middle oxygen atom were chosen as tracer particles to compute transport properties of the TFSI anion and PEO chains, respectively. An in-house code was used to compute ionic conductivity and transport numbers based on the Nernst-Einstein approximation and the Onsager coefficients[29]. The configurations of the systems were stored every 125 ps for analyzing the coordination environments. We made three replicas of each system to analyze the statistical variation of the transport properties. The replica systems were prepared from different initial configurations with Packmol. Finite-size effects were evaluated by studying two systems with concentration r = 0.17 and PEO chain length of 100 monomers of double size.

The glass transition temperature in some selected systems was determined by cooling the systems with 5 K temperature intervals from 288 to 208 K at atmospheric pressure in the NPT ensemble. Each cooling was performed during 2 million time steps, and the temperature was then held constant at each temperature interval for 6 million time steps. The average density was calculated during the final 2 million time steps of each isothermal step. The glass transition temperature was determined from the change of the density as a function of temperature[57,58]. Three replica simulations were performed to determine averages and standard deviations for each system.

The reported values and uncertainties were estimated by calculating the mean and standard deviations of the quantities obtained from the simulations.

4 Results and discussion

The ionic conductivities and ionicities of all systems are presented in Figure 1. The Nernst-Einstein approximations are denoted with superscript NE. n denotes the length of the PEO chains in number of ethylene oxide units. r denotes the salt concentration as defined by the number of Li divided by the number of EO units.

The ionic conductivities of all the systems increase with increasing salt concentration until reaching a maximum around a salt concentration of r = 0.17, corresponding to a fully saturated system (EO:Li = 6) where all ether oxygen atoms coordinate Li. Upon further increasing the salt concentration, the conductivities go down. The systems with shorter PEO chains, n = 23, display higher conductivities due to faster chain dynamics, as expected[61–63]. The glass transition temperatures of the short-chained systems appear to be slightly lower than in the long-chained systems, shown in Table S5 (ESI†), which could partially explain the higher conductivity of the short-chained systems, even though the variation in some systems is substantial. Surprisingly, the ionic conductivities computed from the Onsager coefficients taking ion-ion correlations into account are generally higher than the Nernst-Einstein approximations. This corresponds to ionicities above one, displayed in Figure 1b, meaning that ionic correlations contribute to increasing the conductivity. This is an unexpected observation which we will discuss later.

Experimental ionic conductivities measured by Lascaud *et al.*[59] and Pesko *et al.*[10] are shown in Figure 1a as comparison with the simulated values. Lascaud *et al.* used a PEO polymer with molecular weight M_n, of 3900-4500 g mol^{-1}, which is closest to the n = 100 system, which contains PEO chains with a molecular

View Article Online
DOI: 10.1039/D3NJ04065H

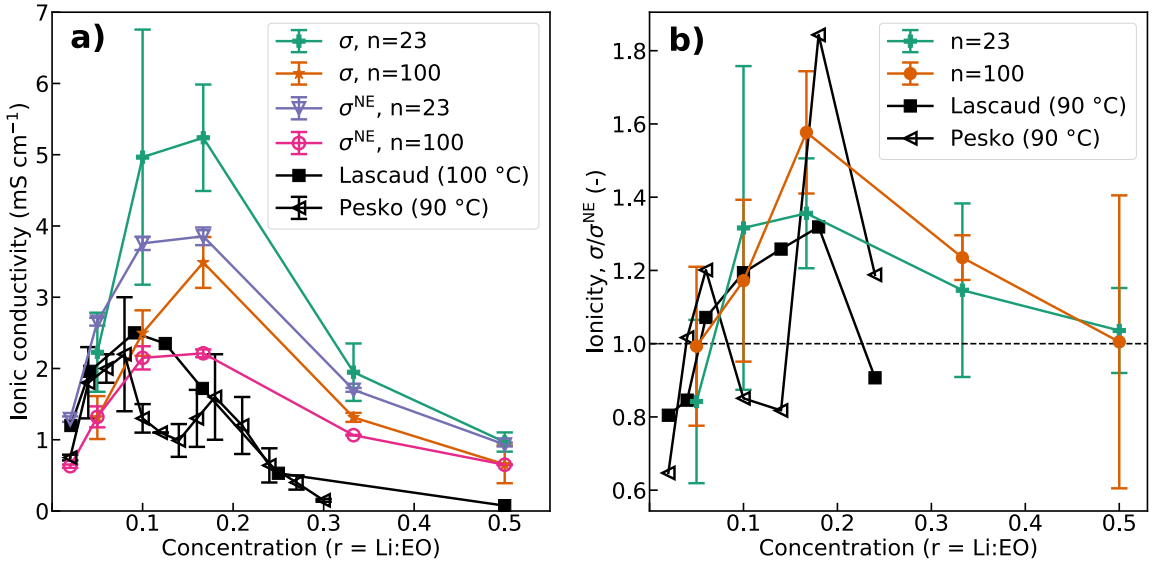

Fig. 1 (a) Ionic conductivity and (b) ionicity of PEO-LiTFSI systems as function of salt concentration and chain length. Experimental ionic conductivities by Lascaud *et al.*[59] measured at 100 °C and Pesko *et al.*[10] measured at 90 °C are shown for comparison. Ionicity = σ/σ^{NE}. The experimental ionicity values are calculated by dividing experimental ionic conductivities measured by electrochemical impedance spectroscopy[10,59] by conductivity values calculated using self-diffusion coefficients (NE approximation) from pulsed-field gradient nuclear magnetic resonance (pfg-NMR) data[9,60].

weight of 4420 g mol^{-1}. The experimental values measured at a temperature of 100 °C are expected to be lower than the simulated values obtained at 150 °C. However, the experimental conductivities are higher than the corresponding simulated values at salt concentrations below r = 0.1. Furthermore, the experimental values by Lascaud *et al.* reach a maximum and start to drop at a lower salt concentration of r = 0.09. At higher salt concentrations, above r = 0.17, the simulated conductivities are higher than the experimental values, as expected. The experimental ionic conductivity measured by Pesko *et al.* follow the same trend as the simulated data, except for a local minimum between r = 0.10 and r = 0.18. Despite these discrepancies, there is relatively good agreement between experimental and computed conductivities, and it seems that the model captures the overall trend of the ionic conductivity.

Figure 2a shows the Li-ion transport numbers computed with the Nernst-Einstein approximation. The NE Li-ion transport numbers are quite low, below 0.3 for all salt concentrations except the highest, and decrease with increasing concentration until reaching a minimum of around 0.1/0.2 in the saturated system (r = 0.17). Apparently, the NE Li-ion transport number increases from r = 0.02 to r = 0.10 for the systems with chain length n = 100 but the error bars are too large in this range to conclude that this is the case. There are few ions in the simulated systems at the lowest concentrations, *e.g.* only 80 salt pairs at r = 0.02, and this increases the uncertainty due to limited data. In the supersaturated salt concentration region above r = 0.17, the NE Li-ion transport numbers increase again for both chain lengths. The polymer electrolytes composed of shorter chains display higher Li-ion transport numbers at all salt concentrations. The simulated NE values in Figure 2a are compared to experimental values from a study by Pesko *et al.*[9], which measured the Li-ion transport number in PEO-LiTFSI electrolytes using pulsed-field gradient nuclear magnetic resonance (pfg-NMR) probing the self-diffusion coefficients of the ions. The simulated values for the systems with chain length n = 100 are converted to steady-state Bruce-Vincent transport numbers using a recent method by Shao and Zhang[65], and they are denoted as $t_{Li^+}^{SS}$ in Figure 2a. These are comparable to experimental values obtained using the steady-state current method developed by Bruce and Vincent[66] from Pesko et al.[10] and Pożyczka et al.[8] on PEO-LiTFSI electrolytes. Hence, Figure 2a compares data from methods for dilute or ideal electrolytes. We do not expect the pfg-NMR and steady-state methods to give equal results, but they are reasonably similar. We observe relatively good agreement between experimental and simulated data in Figure 2a. The overall trend of a low and decreasing Li-ion transport number reaching a minimum at a salt concentration of r = 0.17, after which it increases again for higher salt concentrations, is present in both the experimental and simulated data. For the highest salt concentration, however, there is a significant deviation between the simulated data and experimental data by Pożyczka et al. Also, the steady-state converted simulated transport number for the most dilute system deviates from the experimental data which can be explained by limited data as mentioned above.

Li-ion transport numbers computed using the Onsager coefficients, taking ion-ion correlations into account, are presented in Figure 2b. The Onsager Li-ion transport numbers are quite high, above 0.3 for all salt concentrations, and increase with increasing salt concentration until a maximum value of above 0.6 in the most concentrated systems. There is negligible difference between the systems with short and longer PEO chains. Experimental data for the Li-ion transport numbers using methods for concentrated electrolytes are shown for comparison in Figure 2b. Pesko *et al.*[9]

View Article Online
DOI: 10.1039/D3NJ04065H

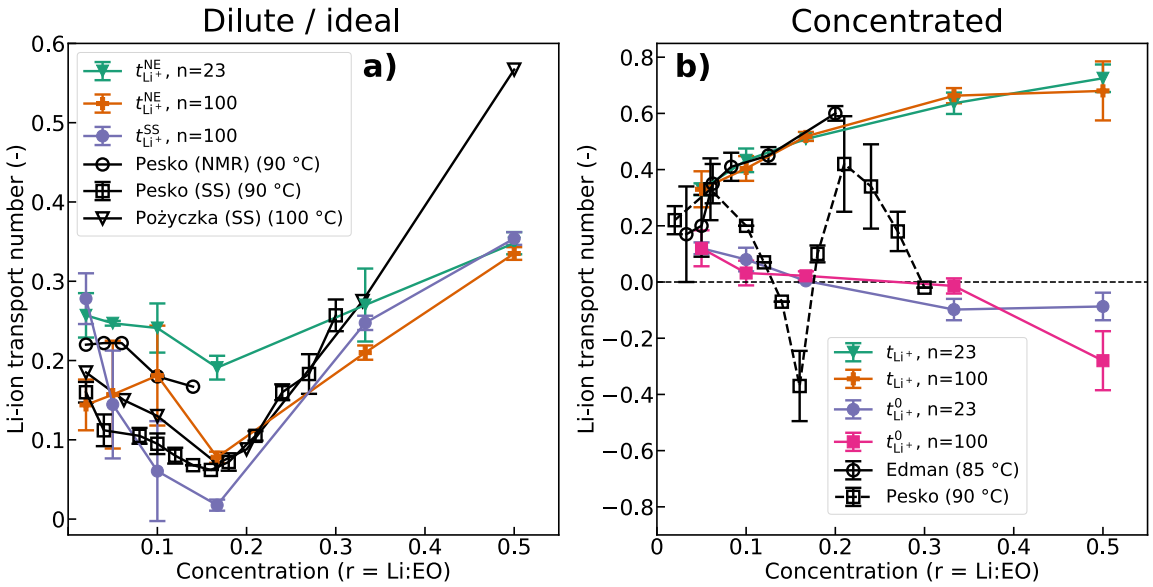

Fig. 2 Computed and experimental transport numbers of PEO-LiTFSI systems as function of salt concentration and PEO chain length. (a) Nernst-Einstein (NE) and steady-state (SS) converted transport numbers compared to pfg-NMR derived transport numbers[9] and experimental steady-state current transport numbers[8,10]. (b) Onsager transport numbers compared to experimental transport numbers from two studies using the Newman methods[10,64]. Onsager transport numbers converted to the solvent velocity reference frame are denoted with superscript 0.

and Edman *et al.*[64] measured the Li-ion transport number in PEO-LiTFSI electrolytes using two slightly different methods based on concentrated solution theory, both developed by Newman and colleagues[10]. The experimental data by Edman *et al.* deviates significantly when compared to the data by Pesko *et al.* for salt concentrations above r = 0.05. The main difference of the experimental work of Pesko and Edman was the length of the PEO chains used to prepare electrolytes. In the work by Pesko *et al.*, they used rather short PEO chains of molecular weight 5 kg mol^{-1}, while Edman and colleagues used high-molecular weight PEO with M_w = 5000 kg mol^{-1}. It is not clear why there are such large differences in the data of Edman and Pesko. The Newman method gives transport numbers in the solvent velocity reference frame while the MD simulations produce transport numbers in the barycentric reference frame. In order to properly compare the simulated and experimental transport numbers in similar reference frames, we converted the computed barycentric transport numbers to the solvent velocity reference frame[67,68] and these are also displayed in Figure 2b. Notably, negative Li-ion transport numbers are observed both in the experimental data by Pesko *et al.* and in the simulated data in the solvent velocity reference frame.

There are significant differences between the rigorously computed transport numbers, obtained with Onsager coefficients, and the Nernst-Einstein approximations. This is a strong indication that ion-ion correlations are important in this system and that the system behaves far from ideally, particularly at higher salt concentrations, when r $\geq$ 0.1. Both experimental and simulated data suggest that the Nernst-Einstein approximation is not valid at higher salt concentrations in this electrolyte system.

Frame of reference

Calculation of transport properties, such as diffusion coefficients and transport numbers, depends on the frame of reference. In our simulations, the center of mass of the particles in the simulation box is used as the frame of reference, *i.e.* the barycentric reference frame. All transport numbers and coefficients in this work are reported in the barycentric frame of reference unless otherwise specified. The computed Onsager transport numbers are compared to experimental data by Pesko *et al.*[10] and Edman *et al.*[64] in Figure 2b. Both of these studies use the Newman method for determining transport numbers, which employ the solvent velocity as the frame of reference[69]. A recent study by Mistry *et al.*[70] reported that the solvent is not static in PEO-LiTFSI polymer electrolytes when a current is passed through, particularly not at higher salt concentrations. The driving force for the solvent motion was indicated to be the diffusion of charged species. By taking the moving electrode/electrolyte interface as the reference frame instead of the solvent velocity, they showed that the cations move in the same direction as the electric current, corresponding to a positive Li-ion transport number, in contrast to previous studies[9,10]. This shows the importance of the choice of reference frame. When the solvent is the major component of a mixture, it is convenient to use it as the reference, but for highly concentrated systems it might not be the proper choice. Considering electrolytes for Li-ion batteries, we are normally interested in the motion of ions relative to the surface of the electrodes. If the center of gravity of the electrolyte is shifting relative to the electrodes during an experiment or practical use, our results might not be directly applicable to describing the transport properties of the electrolyte for use in Li-ion batteries[71]. Recently, Shao *et al.*[68] investigated the importance of reference frame in PEO-LiTFSI polymer electrolytes and also presented a method

View Article Online
DOI: 10.1039/D3NJ04065H

for transforming transport numbers and Onsager coefficients between the barycentric and solvent velocity reference frames. The authors found a reasonable correlation between experimental and simulated transport numbers after transforming the values to the same reference frame. Our results agree well with the results of Shao *et al.*

The analysis and understanding of transport coefficients and transport of species in multi-component mixtures becomes difficult if the motion of the reference frame is unknown. This can be the case for "internal" frames of reference which are part of the system, such as the barycentric or solvent velocity reference frames[71]. The laboratory frame of reference can be viewed as an "external" frame of reference which is outside the system and does not move with respect to an experimental apparatus containing an electrolyte. Therefore, it is convenient for analyzing transport during diffusion experiments[72,73]. The volume-fixed frame of reference is equivalent to the laboratory reference frame when the electrolyte mixture is incompressible, *i.e.* when the partial molar volumes are constant as a function of salt concentration[72,74,75]. Hence, we have converted the barycentric ionic Onsager transport coefficients to the volume-fixed reference frame to support our barycentric data and these will be presented in the next section. Various frames of reference and the transformations between them are further discussed in Refs. 27,76.

To gain a deeper understanding of the ionic conductivities and transport numbers, we computed the Onsager coefficients and self-diffusion coefficients of the components in the systems and they are presented in Figure 3. The self-diffusion coefficients are used to calculate the Nernst-Einstein values, while the Onsager coefficients are related to the Onsager ionic conductivity and transport numbers. The self-diffusion coefficients of all components in Figure 3a decrease with increasing salt concentration. This is in good agreement with several studies[11,62,77] which suggest that the binding of Li-ions to the polymer decreases the polymer flexibility and increases the viscosity, which decreases the self-diffusivity of all components. The self-diffusion coefficients of Li and PEO follow each other quite closely, which is logical given that Li is coordinated by ether oxygen in PEO. The TFSI self-diffusion coefficients are significantly higher than the self-diffusion coefficients of Li and PEO. The simulated self-diffusion coefficients are compared to experimental data by Timachova[60] measured at 90 °C using pfg-NMR. D_{Li} was measured on lithium-containing species and D_{F} was measured on fluorine-containing species. These should be comparable to the self-diffusion coefficients of Li and TFSI obtained from the systems with chain length n = 100. The experimental D_{F} is lower than the simulated D_{TFSI} which is expected considering the lower temperature in the experiment, but both decrease with higher salt concentrations. The experimental D_{Li} is a bit higher than the simulated D_{Li} in the most dilute system, while at the higher concentrations the simulated values are higher, as expected. As mentioned, the limited number of ions in the simulated systems at the lowest concentrations increases the statistical uncertainty. Additionally, the simulated D_{Li} at r = 0.02 was calculated from the sub-diffusive regime. This could explain the unexpectedly low value at the lowest concentration. Apart from the data of the most dilute system, the trend of the simulated data is in good agreement with the experimental values. The trend of the simulated D_{Li} in the sub-saturated region is reflected in the NE Li-ion transport number in Figure 2a.

The barycentric Onsager coefficients in Figure 3b provide information on the ionic correlations in the electrolyte systems. As an example, L_{--} describes the transport of anions in a chemical potential gradient of anions. L_{--} decreases with increasing salt concentration for the systems with chain length n = 100. The corresponding trend for the shorter chain systems is not so clear, particularly for low salt concentrations below r = 0.1 due to the large error bars. L_{++} seems to increase until a maximum at the salt concentration of r = 0.17 and then decrease at higher salt concentrations. This means that the Li-ions move more efficiently in a chemical potential gradient of Li-ions below the super-saturated concentrations than they do in the absence of such a gradient, as described by the self-diffusion coefficient. In the super-saturated region, L_{++} is higher than L_{--} which explains why the Onsager Li-ion transport numbers are above 0.5 in this region. The decreasing L_{--} with higher salt concentrations can be explained by considering the microscopic free volume in the electrolyte. The TFSI anion is believed to move in the free volume between the polymer chains, not directly coordinated by the polymer[78]. As the density of the electrolytes increase with increasing salt concentration, the free volume decreases which results in a reduction of the anion mobility[64]. The density of the systems as function of salt concentration is shown in Figure S1 (ESI†). Interestingly, L_{+-} is negative at all concentrations and reaches a minimum at a salt concentration of r = 0.1-0.2. L_{++} reaching a maximum and L_{+-} reaching a negative minimum at the salt concentration r = 0.17 results in a maximum in the ionic conductivity and ionicity shown in Figure 1a and 1b, respectively. The magnitude of the coupling coefficient L_{+-} is considerable relative to the main coefficients, L_{++} and L_{--}, when compared to common carbonate-based battery electrolytes[33]. However, the relation $L_{ii}L_{jj} \geq L_{ij}^2$[27] holds for all systems. The trend of the ionic conductivity is a consequence of the balance between the number of free charge carriers and their mobility, which is tightly coupled to the polymer segmental motion, as shown in several studies[25,79–81]. Shao and Gudla et al. also found negative L_{+-} values in PEO-LiTFSI electrolytes in the barycentric frame of reference[68,82]. Negative L_{+-} values mean that the cation-anion correlation contributes to increasing the ionic conductivity of the system[83], resulting in ionicities above 1. This is a counter-intuitive result. Firstly, it indicates that in this model, the TFSI anions bond weakly to the Li-ions, which we can justify given the bulky size of the TFSI anion and its highly delocalized charge[3,81]. Secondly, the TFSI anion is known to plasticize the polymer, *i.e.* increase polymer flexibility[3]. Hartree-Fock calculations have shown that the energy barrier for rotation about the S−N bonds in TFSI is comparable to the barriers for rotations of the C−C and C−O bonds in diglyme[84,85]. The corresponding dihedral interactions describing rotations in TFSI and PEO in the model we used are of similar magnitude. The plasticizing nature of the TFSI could thus facilitate and increase the Li-ion diffusion. In addition, it could increase diffusion of TFSI itself because enhanced polymer chain flexibility will create more voids for the anion to move into. The TFSI anion is illustrated in

View Article Online
DOI: 10.1039/D3NJ04065H

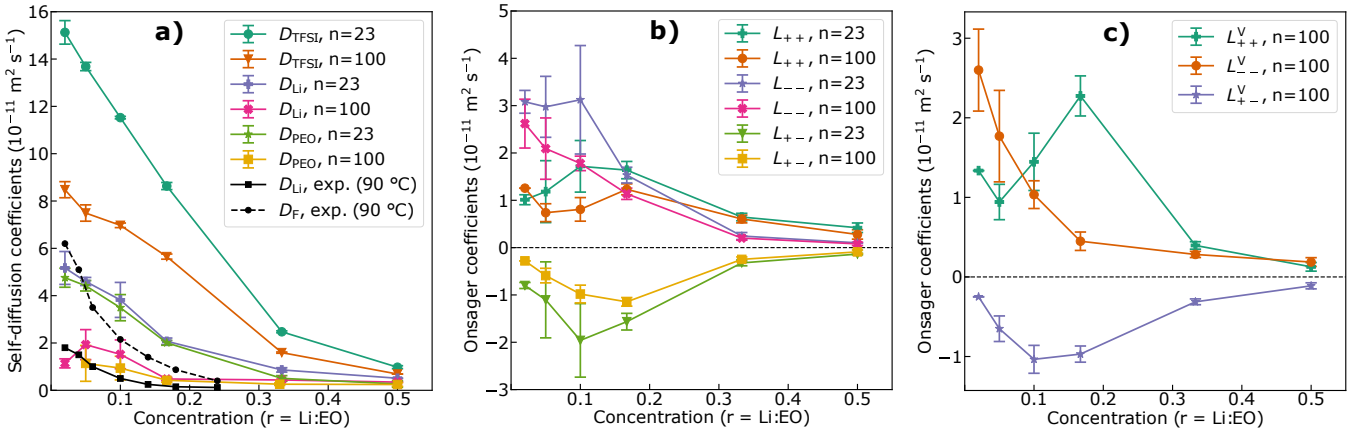

Fig. 3 (a) Self-diffusion coefficients, (b) Onsager coefficients in the barycentric reference frame, and (c) Onsager coefficients in the volume-fixed reference frame as function of salt concentration and chain length. The error in the volume-fixed coefficients was calculated using uncertainty propagation rules. Experimental self-diffusion coefficients by Timachova[60]. The self-diffusion coefficient of Li in the n = 100 system did not fully reach the diffusive regime at salt concentrations of r = 0.02, 0.05 and 0.10. The self-diffusion coefficient of PEO in the n = 100 system did not fully reach the diffusive regime at salt concentrations of r = 0.02, 0.05, 0.10, 0.33 and 0.50. L_{++} and L_{+-} for the n = 100 and r = 0.02 system were obtained in just one simulation and therefore have no error bars.

Figure S2 (ESI†). Notably, the L_{+-} reaches a negative minimum at a quite high salt concentration (r = 0.1-0.2). The plasticization effect apparently increases with increasing salt concentration up to the saturated system due to the higher number of anions. At even higher concentrations, the effect is diminished which again reduces the ionicity. Ionicity values above one are rarely encountered in the literature, but they are not impossible[79,86,87]. The ionicity as a function of salt concentration calculated from experimental data for PEO-LiTFSI electrolytes is displayed in Figure 1b and S3 (ESI†), and ionicities above one are evident for some salt concentrations, see also Ref. [87]. In electrolyte systems with shorter chains, *e.g.* triglyme or tetraglyme and LiTFSI salt, ionicity values below one have been found[88,89]. This suggests a change of the microscopic transport mechanisms and the significance of the cation-anion correlation upon increasing the chain length from glymes to PEO. It is also worth noting that in coarse-grained MD simulations of polymer electrolytes with monomers and ions described as spherical beads, ionicity values above one have not been observed[80,81], which suggests that atomic resolution is necessary to detect this phenomenon.

The barycentric Onsager coefficients for the systems with long PEO chains were converted to the volume-fixed reference frame using the method explained in Refs. [68,73,74,76], and these are shown in Figure 3c. The partial molar volumes of the components are required to perform the conversion and these were obtained using Kirkwood-Buff integrals and the expressions of Ruckenstein and Shulgin[90]. The trends and values of the volume-fixed Onsager coefficients are mostly similar as the barycentric coefficients. Notably, the L_{+-} values are negative also in the volume-fixed reference frame. The partial molecular volumes of the neutral components, shown in Figure S7 (ESI†), do not change dramatically with concentration which indicates that the assumption of incompressibility is acceptable. The volume-fixed Onsager coefficients are thus relevant also in an external frame of reference which supports our above argument concerning the barycentric Onsager coefficients. We note that the Li-ion transport number in the volume-fixed frame of reference display the same trend as in the barycentric frame of reference, shown in Figure 2b.

We cannot avoid mentioning that the above findings contradict much of the literature published on this system which indicate that Li and TFSI tend to form mobile negatively charged clusters, *e.g.* two TFSI connected to one Li[9,10,20,69,91]. The two anions then drag the Li-ion away from the cathode towards the anode during discharge which causes negative Li-ion transport numbers. The remaining Li-ions not present in anion-dominated clusters are believed to be rather immobile compared to the clusters. This behavior does not seem to occur in our models. The Onsager coefficients involving the solvent (PEO) are presented in Figure S4 (ESI†). We calculated the Maxwell-Stefan coefficients from the Onsager coefficients using the method developed by Krishna et al.[92] and they are displayed in Figure S5 (ESI†). Transport properties for some selected systems were simulated at a reduced temperature of 353 K and these are shown in Table S4. The trends of the transport coefficients did not change dramatically compared to the simulations at 423 K, only their magnitudes due to slower dynamics.

We analyzed the average static coordination environments around Li by computing the radial distribution functions and coordination numbers of Li and ether oxygen and Li and the central nitrogen of TFSI anions. The resulting plots for the Li-ether oxygen and Li-TFSI nitrogen coordination are presented in Figure S6 (ESI†) and Figure 4, respectively. More coordination data are presented in Table S3 (ESI†). Li is coordinated by 5 to 6 ether oxygen at salt concentrations up to r = 0.17. The RDFs for Li-TFSI show little sign of ion pairing closer than 5 Å for the concentrations lower than r = 0.17. This observation is in line with several spectroscopic and diffraction studies[7,93–95]. At the saturated concentration, r = 0.17, there is some indication of ion pairing and at higher concentrations there are clear signs of ion association. At the concentration r = 0.50, every Li is coordinated by more

View Article Online
DOI: 10.1039/D3NJ04065H

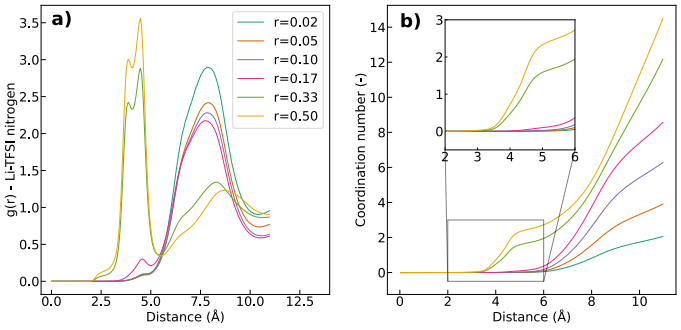

Fig. 4 (a) Radial distribution functions and (b) coordination numbers of Li and TFSI nitrogen for the different salt concentrations with chain length n = 100.

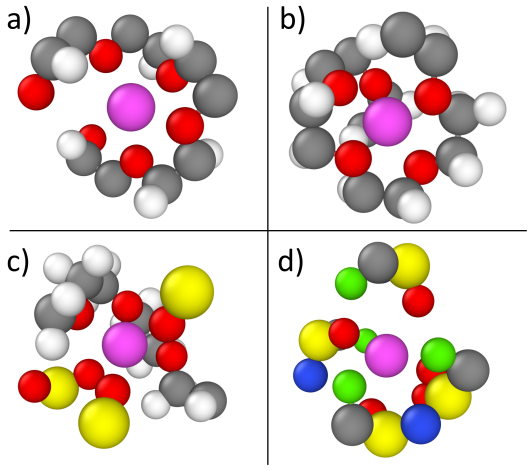

Fig. 5 Snapshots of Li coordination environments obtained with Ovito[96]. (a) Li coordinated by six ether oxygen, r = 0.17. (b) Li coordinated by five ether oxygen, r = 0.17. (c) Li coordinated by three ether oxygen and three oxygen from two TFSI anions, r = 0.33. (d) Li coordinated by oxygen from three TFSI anions, r = 0.50. Colors: Carbon is grey, oxygen is red, hydrogen is white, sulphur is yellow, nitrogen is blue, fluorine is green and lithium is purple.

than two TFSI anions on average, meaning that ion clusters form throughout the material. Consequently, the average coordination number of ether oxygen is reduced to less than 2.5, as shown in Figure S6b (ESI†). The total coordination number of oxygen is maintained at 5 to 6 but fluorine contacts are also observed in the super-saturated systems. Examples of Li coordination environments during the simulations are displayed in Figure 5.

To obtain a better understanding of the significance of the coordination environment, it is necessary to examine the dynamic nature of the coordination[82]. We evaluated the dynamic properties of the coordination environments of Li by calculating the residence times of Li-ether oxygen, Li-PEO chain, and Li-TFSI nitrogen for the different salt concentrations and PEO chain lengths. The residence time is an estimate of the time that a pair of two species stay within a certain cutoff distance, as neighbors, before parting ways. Figure 6 displays the average residence times.

The residence times of Li-ether oxygen and Li-PEO chain obviously follow the same trend. The Li-ether oxygen residence times are generally shorter than the Li-PEO chain residence times be-

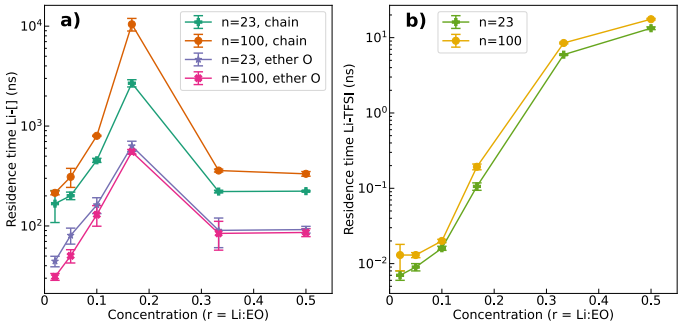

Fig. 6 Estimated average residence times for (a) Li-ether oxygen and Li-PEO chain and (b) Li-TFSI as function of salt concentration and chain length. Note logarithmic scale on the y axis. Note that some of the calculated residence times, particularly of Li-PEO chain, are much longer than the total simulation time. They might be more uncertain than reflected in the standard deviations (error bars), but we believe that the main trend of the data should hold.

cause Li normally moves a distance along a chain before jumping to the next chain. There is little dependence of chain length on the Li-ether oxygen residence times but the Li-ions sit slightly longer with the ether oxygen in the shorter chains than in the longer chains. The residence times of Li-ether oxygen are between 30 and 600 ns, indicating strong ion-solvent coordination. The residence times increase dramatically with increasing salt concentration until reaching a maximum in the saturated systems at concentration of r = 0.17. At higher salt concentrations, the residence times decrease again. As the Li concentration increases from the most dilute system, more ether oxygen atoms become coordinated to Li and fewer ether oxygen are uncoordinated/free. This increases the residence time as it becomes less likely for Li to find and jump to a free ether oxygen site. In the saturated system, at r = 0.17, all ether oxygen are in principle occupied and the residence time reaches a maximum. Li jumps must then occur by nearly all the Li jumping simultaneously in a collective manner which is a low-probability event. In the super-saturated systems, some Li are partly coordinated to anions and they can possibly move more freely between ether oxygens and PEO chains. This decreases the average residence time. The Li that only are coordinated to ether oxygen should still exhibit long residence times, leading us to believe there could be a distribution of residence times in these systems.

To investigate this, we calculated the distribution of the pair lifetime correlation function for some selected systems at selected time intervals. The results for the system with longer PEO chains and the highest salt concentration are presented as violin plots in Figure 7. Mean and extreme values are indicated in the violin plots. The mean values correspond to the pair lifetime correlation used to calculate average residence times in Figure 6. The maximum and minimum values correspond to the individual pairs of Li-ether oxygen, Li-PEO chain, or Li-TFSI that exhibit the longest and shortest neighbor times, respectively. Wide pair lifetime correlation function distributions are observed for Li-ether oxygen and Li-PEO chain in the super-saturated system r = 0.50, supporting our hypothesis that some Li move quickly between ether oxygen atoms and PEO chains while others stay at the same site

View Article Online
DOI: 10.1039/D3NJ04065H

for much longer times. The bimodal distributions of Li-PEO chain indicates that some Li are coordinated to the same chain during the entire simulation time while others jump between chains more frequently. We also observe wide distributions in the other systems, particularly those close to the saturated concentration of r = 0.17, presented in Figure S8 and S9 (ESI†). Even if the average Li-ether oxygen and Li-PEO chain residence time at the salt concentrations r = 0.05 and r = 0.33/0.50 are quite similar, the distributions are wider in the super-saturated systems than the sub-saturated system. This is an indication that the Li are changing coordination by different mechanisms in the different systems. We calculated the average number of anions coordinated to the Li exhibiting the longest and shortest Li-ether oxygen and Li-PEO chain residence times in Figure 7. Details of the calculation are given in the SI. The Li displaying weaker correlation to ether oxygen and PEO chain, *i.e.* shorter residence times, were on average coordinated to more anions than the Li displaying stronger correlation to ether oxygen and PEO chain, *i.e.* longer residence times. Furthermore, the Li with shorter residence times (coordinated by more anions) moved faster and further than the Li with longer residence times (coordinated by fewer anions) in the most concentrated systems, see Table S8 (ESI†). This observation suggests that the Li-TFSI interaction facilitates Li jumps between ether oxygen and between PEO chains, which is in line with the negative L_{+-} in Figure 3, meaning that the Li-TFSI correlation contributes to enhancing the Li transport and hence the ionic conductivity. Shen and Hall also hypothesized that the cation-anion interactions could increase diffusion in polymer electrolytes in specific situations[80]. The finding is however in contrast to the study by Molinari et al.[20] in which Li coordinated to more anions exhibited lower mobility. The systems with concentrations lower than r = 0.33 exhibit smaller differences with respect to anion coordination of the Li that are stronger and weaker correlated to ether oxygens and PEO chains, likely due to the generally low anion coordination numbers in these systems. The results are summarized in Table S7, S8 and S9 (ESI†). The above analysis shows that the average residence time can hide interesting information about the distribution of pair lifetimes and generally about the dynamics of a system.

Notably, the systems with the longest residence time of Li to ether oxygen and PEO chain, at concentration r = 0.17, are also the systems with the highest ionic conductivity, see Figure 1. A substantial contribution of the Li transport must then come from vehicular diffusion with the PEO chains. In fact, vehicular diffusion represents a significant part of the Li transport in all the systems, in agreement with previous studies[61,81]. The root-mean-square diffusion length of Li between each change of ether oxygen coordination can be estimated using the Einstein-Smoluchowski equation[12]:

$$\lambda_{\mathrm{Li}} = \sqrt{6 D_{\mathrm{Li}} \tau_{\mathrm{Li-etherO}}}, \qquad (15)$$

where D_{Li} is the self-diffusion coefficient of Li and $\tau_{\mathrm{Li-etherO}}$ is the average residence time of Li and ether oxygen. The mean diffusion length of Li between changing ether oxygen coordination is presented in Figure S11 (ESI†). Longer mean diffusion lengths indicate that vehicular diffusion dominates the transport. As shown in Figure S11, vehicular diffusion becomes more important with increasing salt concentration from the dilute systems to the saturated system. The drastic reduction of mean diffusion length in the super-saturated systems is due to significantly slower dynamics and a shift from vehicular to structural diffusion. The Einstein-Smoluchowski equation is based on the three-dimensional random walk which might not be correct at all concentrations in these systems. However, the trend of the data appears plausible.

The residence times of Li and TFSI as function of salt concentration and PEO chain length are shown in Figure 6b. For the most dilute systems, the residence times are very short, below 20 ps, indicative of very limited ion pairing. Upon increasing the concentration from r = 0.10 to 0.33, the residence time increases by about two orders of magnitude. At the highest concentrations, r = 0.33 and 0.50, Li-TFSI pairs are present and relatively long-lived, with a residence time on the order of 10 ns. During this time period, Li and TFSI acts as an electroneutral unit which does not carry electric charge. Combined with the decline of absolute values of the Onsager coefficients at the highest concentrations, this results in a decrease of ionic conductivity in the super-saturated regime, seen in Figure 1a. From Figure 7c we observe that some Li-TFSI pairs are stronger correlated, *i.e.* longer-lived, than the average and they will contribute more to reducing the ionic conductivity. The residence time at the concentration r = 0.17 is about 0.1 to 0.2 ns, too short to significantly influence the ionic conductivity.

The thermodynamic factor of the systems with chain length n = 100 calculated according to equation (14) are presented in Figure 8. A thermodynamic factor of one indicates an ideal mixture, and values away from one indicate non-ideality. Upon extrapolation to the dilute limit, r = 0, the thermodynamic factor approaches one as expected. The system becomes more non-ideal with increasing concentration, reaching a maximum in the saturated system, at r = 0.17. The thermodynamic factor is reduced to below one in the super-saturated systems indicating a change of the structure and interactions between the species, which corresponds to our previous discussions on the super-saturated systems. The data support our previous statement that PEO-LiTFSI electrolytes are generally non-ideal systems, even at quite low salt concentrations, most likely due to strong ion-ion correlations. The thermodynamic factor has been measured experimentally and calculated previously using simulations[25,91,97]. Our results agree reasonably well with the experimental data, also presented in Figure 8, except for the highest concentrations where experimental data is lacking.

Deviations between experimental and simulated data

The deviation between the simulated ionic conductivity and experimental values warrants some discussion. In the simulations, the system with concentration r = 0.17 exhibits the highest ionic conductivity, while the experimental data suggest that the ionic conductivity is lower at this concentration than at r = 0.1. Obviously, there are substantial differences between simulations and experiments. Measuring ionic conductivity experimentally is usually done by performing electrochemical impedance spectroscopy

View Article Online
DOI: 10.1039/D3NJ04065H

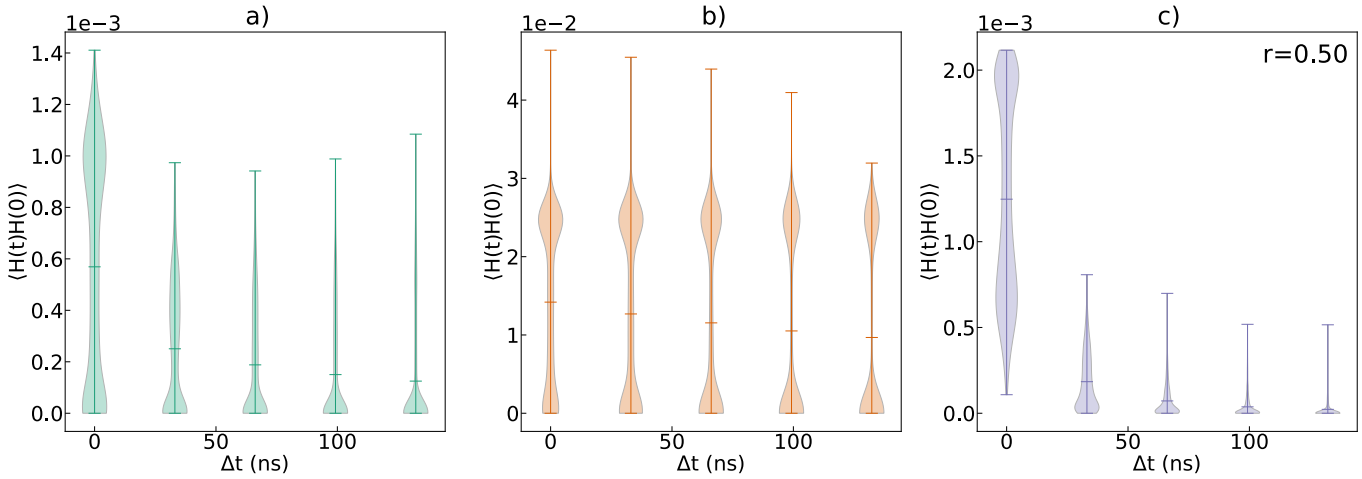

Fig. 7 Distribution of pair lifetime correlation functions at selected time intervals for (a) Li-ether oxygen, (b) Li-PEO chain, and (c) Li-TFSI for the system with chain length n = 100 and salt concentration r = 0.5. Mean and extreme values are marked in the violin plots.

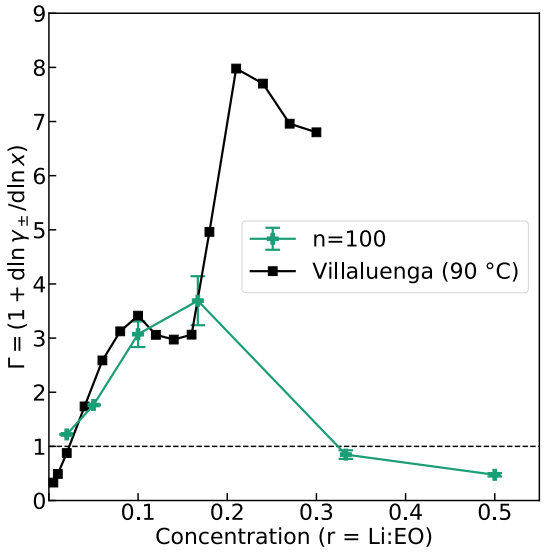

Fig. 8 Thermodynamic factor, Γ, of PEO-LiTFSI as function of salt concentration in the systems with chain length n = 100. Experimental values by Villaluenga et al.[25,91].

on a sample of the electrolyte sandwiched between two blocking electrodes. Hence, interface effects might play a role. In our simulations, the systems are infinite with no interfaces. Furthermore, impurities and defects present in all real materials can influence experimental results, but are non-existent in the simulated systems. The fully saturated system where all ether oxygen are coordinated to Li is possibly a fragile system where local super-saturation and ion clustering might easily occur to create inhomogeneities, for example at interfaces[98]. This could explain the discrepancy between the simulated and experimental values. Additionally, it is possible that our charge-scaled non-polarizable model underestimates the degree of Li-TFSI ion pairing at the saturated concentration[93], r = 0.17, which could result in too high ionic conductivity. Another possible explanation is finite-size effects, as the ionic conductivity at r = 0.17 was lower in a system of double size. The finite-size effects are presented in Table S2 (ESI†).

Li-ions acting as transient crosslinks between different PEO chains can reduce the polymer flexibility and decrease ionic conductivity[62,77]. The majority of Li-ions in our models are coordinated to just one PEO chain (Table S3, ESI†), limiting this effect. Several studies indicate that Li-ions prefer to coordinate to two PEO chains if possible[11,18,99]. Any lack of transient crosslinking in our systems compared to real-world electrolyte might cause the ionic conductivity to be artificially high. However, we believe this should not influence the main findings of the work.

Even though much work has been done to develop polymer electrolytes with improved transport properties, PEO-LiTFSI still exhibits some of the highest total and Li^+ partial conductivities of all polymer electrolytes[100]. We have proposed that the molecular character of the TFSI anion is important in PEO-based electrolytes and facilitates the transport of Li^+ by improving polymer segmental mobility. The LiTFSI salt reduces the crystallinity of neat PEO, making it more amorphous and increasing the chain flexibility. Electronic structure calculations suggest that the rotational flexibility around the S−N bonds is the main cause for this special behavior[84,85]. However, the size, shape and chemical

View Article Online
DOI: 10.1039/D3NJ04065H

character of TFSI could also contribute to breaking the crystalline domains of PEO and enhancing its flexibility. Compared to many anions, TFSI clearly has unique properties and interact with PEO in a favorable way[3]. Nonetheless, other anions could potentially improve the transport properties of PEO-based electrolytes even further. Alternative polymer host materials with different chemical character than PEO could also potentially benefit from using salts with other anions than TFSI[100]. The cation-polymer interaction and coordination has been thoroughly studied in many polymer electrolytes[101,102]. We believe that a deeper understanding of the cation-anion and anion-polymer interactions are also useful for the development of next-generation polymer electrolytes and more effort should be directed towards engineering and developing new anions.

5 Conclusion

In this work, we have computed charge transport properties of PEO-LiTFSI polymer electrolytes, *i.e.* ionic conductivity and transport numbers, by equilibrium MD simulations. The results are comparable to experimental data, indicating that our models describe the real systems well. The values obtained using the NE approximation and Onsager coefficients and the significant differences between the results from the two methods suggest that the systems are non-ideal, which is further supported by our computation of thermodynamic factors. Therefore, we believe that determination of Onsager coefficients is necessary to understand the transport properties of these systems. Notably, negative L_{+-} values mean that Li and TFSI are anticorrelated, *i.e.* that their correlation contributes to increasing the ionic conductivity. This results in ionicity values above one, so-called superionicity. We attribute this effect to the rotational flexibility of the TFSI anion which plasticizes the PEO chains, facilitating Li transport. We observe that the Onsager coefficients L_{+-} and L_{++} reach absolute maxima at salt concentrations between r = 0.10 and r = 0.17, corresponding to maximum ionic conductivity and ionicity. The self-diffusivities, on the other hand, decrease monotonically with increasing salt concentration. Onsager coefficients converted to the volume-fixed reference frame agree well with the barycentric values obtained from simulations. The sum of the partial molar volumes of the components does not change much with increasing salt concentration, meaning that the volume-fixed frame of reference can be related to an external reference frame; the laboratory frame of reference. Both the volume-fixed and the barycentric frames of reference apparently move little relative to an external reference frame which simplifies the analysis of the Onsager transport coefficients. The absolute value of the coupling coefficient L_{+-} is remarkably large compared to the main coefficients, meaning that the cation-anion coupling is important in these electrolytes. The static and dynamic properties of the Li coordination environments were studied to understand the transport mechanisms of Li-ions. Very limited Li-TFSI ion pairing is observed for salt concentrations lower than r = 0.17. At the saturated concentration, r = 0.17, some Li-TFSI ion-pairing is observed but the residence time is too short to significantly influence the ionic conductivity. In the super-saturated systems, relatively long-lived ion-clusters are present throughout the material. The residence times of Li-ether oxygen and Li-PEO chains vary considerably with salt concentration, and are indeed very long at the saturated concentration, indicating that vehicular diffusion dominates the transport of Li. We observe a dramatic reduction of these residence times in the super-saturated systems, suggesting a change from vehicular to structural diffusion. The distribution of residence times provides more information on the variation of the dynamic properties of the Li environments. Bimodal distributions suggest that some Li quickly change coordination while others stay at the same site for longer times. The Li that display faster intrachain (Li-ether oxygen) and interchain (Li-PEO chain) jumps in the super-saturated systems are coordinated to more anions than the Li that are more strongly correlated to the coordination sites. This finding agrees well with the observation of negative L_{+-} values. We believe this implies that the TFSI anions facilitate Li jumps and Li transport, enhancing Li-ion conduction and the Li-ion transport number. Generally, we believe the anion is important for the transport properties of polymer electrolytes and a better understanding of its role in the charge transport is necessary.

The discrepancies that we observe between simulated and experimental data are discussed. Simulations and experiments are unavoidably fundamentally different and direct comparison between their results warrants caution and understanding of the inherent differences. One example is the frame of reference used to determine transport numbers, which is often different in experiments and in simulations. Nonetheless, we do believe our results are representative of real PEO-LiTFSI polymer electrolytes for use in Li-ion batteries and that the results will contribute to improved understanding of this fascinating class of materials.

Conflicts of interest

There are no conflicts to declare.

Acknowledgements

The simulations were performed on resources provided by Sigma2 - the National Infrastructure for High Performance Computing and Data Storage in Norway through the projects NN9264K and NN9414K, and on the NTNU IDUN/EPIC computing cluster. The Research Council of Norway is acknowledged for the support to the Norwegian Micro- and Nano-Fabrication Facility, NorFab, project number 295864. SKS acknowledges support through the NRC project 275754.

Notes and references

1 D. Fenton, J. Parker and P. Wright, *Polymer*, 1973, **14**, 589.
2 P. V. Wright, *Br. Polymer J.*, 1975, **7**, 319–327.
3 H. Zhang, C. Liu, L. Zheng, F. Xu, W. Feng, H. Li, X. Huang, M. Armand, J. Nie and Z. Zhou, *Electrochimica Acta*, 2014, **133**, 529–538.
4 M. Armand, *Solid State Ionics*, 1983, **9-10**, 745–754.
5 M. Armand, W. Gorecki and R. Andreani, *Proceedings of the 2nd International Meeting on Polymer Electrolytes*, 1989.
6 Z. Xue, D. He and X. Xie, *J. Mater. Chem. A*, 2015, **3**, 19218–19253.

View Article Online
DOI: 10.1039/D3NJ04065H

7 G. Mao, M.-L. Saboungi, D. L. Price, M. B. Armand and W. S. Howells, *Phys. Rev. Lett.*, 2000, **84**, 5536–5539.
8 K. Pożyczka, M. Marzantowicz, J. Dygas and F. Krok, *Electrochimica Acta*, 2017, **227**, 127–135.
9 D. M. Pesko, K. Timachova, R. Bhattacharya, M. C. Smith, I. Villaluenga, J. Newman and N. P. Balsara, *J. Electrochem. Soc.*, 2017, **164**, E3569–E3575.
10 D. M. Pesko, S. Sawhney, J. Newman and N. P. Balsara, *J. Electrochem. Soc.*, 2018, **165**, A3014–A3021.
11 D. Diddens, A. Heuer and O. Borodin, *Macromolecules*, 2010, **43**, 2028–2036.
12 B. Dereka, N. H. C. Lewis, Y. Zhang, N. T. Hahn, J. H. Keim, S. A. Snyder, E. J. Maginn and A. Tokmakoff, *J. Am. Chem. Soc.*, 2022, **144**, 8591–8604.
13 D. Frenkel and B. Smit, *Understanding Molecular Simulation (Second Edition)*, Academic Press, San Diego, 2002.
14 M. Ebadi, T. Eriksson, P. Mandal, L. T. Costa, C. M. Araujo, J. Mindemark and D. Brandell, *Macromolecules*, 2020, **53**, 764–774.
15 L. J. A. Siqueira and M. C. C. Ribeiro, *J. Chem. Phys.*, 2006, **125**, 214903.
16 A. France-Lanord, Y. Wang, T. Xie, J. A. Johnson, Y. Shao-Horn and J. C. Grossman, *Chem. Mater.*, 2020, **32**, 121–126.
17 D. J. Brooks, B. V. Merinov, W. A. Goddard, B. Kozinsky and J. Mailoa, *Macromolecules*, 2018, **51**, 8987–8995.
18 O. Borodin and G. D. Smith, *Macromolecules*, 2006, **39**, 1620–1629.
19 L. T. Costa and M. C. C. Ribeiro, *J. Chem. Phys.*, 2007, **127**, 164901.
20 N. Molinari, J. P. Mailoa and B. Kozinsky, *Chem. Mater.*, 2018, **30**, 6298–6306.
21 K. D. Fong, J. Self, B. D. McCloskey and K. A. Persson, *Macromolecules*, 2021, **54**, 2575–2591.
22 H. Gudla, C. Zhang and D. Brandell, *J. Phys. Chem. B*, 2020, **124**, 8124–8131.
23 K. D. Fong, H. K. Bergstrom, B. D. McCloskey and K. K. Mandadapu, *AIChE J.*, 2020, **66**, e17091.
24 C. Y. Son and Z.-G. Wang, *J. Chem. Phys.*, 2020, **153**, 100903.
25 Y. Choo, D. M. Halat, I. Villaluenga, K. Timachova and N. P. Balsara, *Prog. Polymer Sci.*, 2020, **103**, 101220.
26 X. Liu, S. K. Schnell, J.-M. Simon, D. Bedeaux, S. Kjelstrup, A. Bardow and T. J. H. Vlugt, *J. Phys. Chem. B*, 2011, **115**, 12921–12929.
27 S. Kjelstrup and D. Bedeaux, *Non-Equilibrium Thermodynamics of Heterogeneous Systems*, World Scientific, Singapore, 2008.
28 K. D. Fong, J. Self, K. M. Diederichsen, B. M. Wood, B. D. McCloskey and K. A. Persson, *ACS Central Sci.*, 2019, **5**, 1250–1260.
29 Ø. Gullbrekken, I. T. Røe, S. M. Selbach and S. K. Schnell, *J. Phys. Chem. B*, 2023, **127**, 2729–2738.
30 V. Bocharova and A. P. Sokolov, *Macromolecules*, 2020, **53**, 4141–4157.
31 W. Zhao, F. Leroy, B. Heggen, S. Zahn, B. Kirchner, S. Balasubramanian and F. Müller-Plathe, *J. Am. Chem. Soc.*, 2009, **131**, 15825–15833.
32 Y. Zhang and E. J. Maginn, *J. Phys. Chem. Lett.*, 2015, **6**, 700–705.
33 S. Kjelstrup, A. F. Gunnarshaug, Ø. Gullbrekken, S. K. Schnell and A. Lervik, *J. Chem. Phys.*, 2023, **159**, 034104.
34 S. K. Schnell, P. Englebienne, J.-M. Simon, P. Krüger, S. P. Balaji, S. Kjelstrup, D. Bedeaux, A. Bardow and T. J. Vlugt, *Chem. Phys. Lett.*, 2013, **582**, 154–157.
35 P. Krüger, S. K. Schnell, D. Bedeaux, S. Kjelstrup, T. J. H. Vlugt and J.-M. Simon, *J. Phys. Chem. Lett.*, 2013, **4**, 235–238.
36 P. G. Kusalik and G. N. Patey, *J. Chem. Phys.*, 1987, **86**, 5110–5116.
37 A. Ben-Naim, *Molecular theory of solutions*, OUP Oxford, 2006.
38 X. Liu, S. K. Schnell, J.-M. Simon, P. Krüger, D. Bedeaux, S. Kjelstrup, A. Bardow and T. J. H. Vlugt, *Int. J. Thermophys.*, 2013, **34**, 1169–1196.
39 A. P. Thompson, H. M. Aktulga, R. Berger, D. S. Bolintineanu, W. M. Brown, P. S. Crozier, P. J. in 't Veld, A. Kohlmeyer, S. G. Moore, T. D. Nguyen, R. Shan, M. J. Stevens, J. Tranchida, C. Trott and S. J. Plimpton, *Comp. Phys. Comm.*, 2022, **271**, 108171.
40 W. L. Jorgensen, J. D. Madura and C. J. Swenson, *J. Am. Chem. Soc.*, 1984, **106**, 6638–6646.
41 W. L. Jorgensen and J. Tirado-Rives, *Proc. National Acad. Sci.*, 2005, **102**, 6665–6670.
42 L. S. Dodda, J. Z. Vilseck, J. Tirado-Rives and W. L. Jorgensen, *J. Phys. Chem. B*, 2017, **121**, 3864–3870.
43 L. S. Dodda, I. Cabeza de Vaca, J. Tirado-Rives and W. L. Jorgensen, *Nucleic Acids Research*, 2017, **45**, W331–W336.
44 K. P. Jensen and W. L. Jorgensen, *J. Chem. Theory Comput.*, 2006, **2**, 1499–1509.
45 J. N. Canongia Lopes and A. A. H. Pádua, *J. Phys. Chem. B*, 2004, **108**, 16893–16898.
46 A. I. Jewett, D. Stelter, J. Lambert, S. M. Saladi, O. M. Roscioni, M. Ricci, L. Autin, M. Maritan, S. M. Bashusqeh, T. Keyes, R. T. Dame, J.-E. Shea, G. J. Jensen and D. S. Goodsell, *J. Mol. Biol.*, 2021, **433**, 166841.
47 J.-P. Ryckaert, G. Ciccotti and H. J. Berendsen, *J. Comput. Phys.*, 1977, **23**, 327–341.
48 R. W. Hockney and J. W. Eastwood, *Computer simulation using particles*, Bristol: Hilger, 1988.
49 I. Leontyev and A. Stuchebrukhov, *Phys. Chem. Chem. Phys.*, 2011, **13**, 2613–2626.
50 L. Martinez, R. Andrade, E. G. Birgin and J. M. Martinez, *J. Comput. Chem.*, 2009, **30**, 2157–2164.
51 W. Shinoda, M. Shiga and M. Mikami, *Phys. Rev. B*, 2004, **69**, 134103.
52 W. G. Hoover, *Phys. Rev. A*, 1985, **31**, 1695–1697.
53 S. Nosé, *Mol. Phys.*, 1984, **52**, 255–268.

View Article Online
DOI: 10.1039/D3NJ04065H

54 T. C. Beutler, A. E. Mark, R. C. van Schaik, P. R. Gerber and W. F. van Gunsteren, *Chem. Phys. Lett.*, 1994, **222**, 529–539.
55 S. H. Jamali, L. Wolff, T. M. Becker, M. de Groen, M. Ramdin, R. Hartkamp, A. Bardow, T. J. H. Vlugt and O. A. Moultos, *J. Chem. Inf. Model.*, 2019, **59**, 1290–1294.
56 J.-M. Simon, P. Krüger, S. K. Schnell, T. J. H. Vlugt, S. Kjelstrup and D. Bedeaux, *J. Chem. Phys.*, 2022, **157**, 130901.
57 J. Han, R. H. Gee and R. H. Boyd, *Macromolecules*, 1994, **27**, 7781–7784.
58 K.-q. Yu, Z.-s. Li and J. Sun, *Macromol. Theory Simulations*, 2001, **10**, 624–633.
59 S. Lascaud, M. Perrier, A. Vallee, S. Besner, J. Prud'homme and M. Armand, *Macromolecules*, 1994, **27**, 7469–7477.
60 K. Timachova, *PhD thesis*, University of California, Berkeley, 2018.
61 D. Devaux, R. Bouchet, D. Glé and R. Denoyel, *Solid State Ionics*, 2012, **227**, 119–127.
62 K. Timachova, H. Watanabe and N. P. Balsara, *Macromolecules*, 2015, **48**, 7882–7888.
63 M. P. Rosenwinkel, R. Andersson, J. Mindemark and M. Schönhoff, *J. Phys. Chem. C*, 2020, **124**, 23588–23596.
64 L. Edman, M. M. Doeff, A. Ferry, J. Kerr and L. C. De Jonghe, *J. Phys. Chem. B*, 2000, **104**, 3476–3480.
65 Y. Shao and C. Zhang, *J. Chem. Phys.*, 2023, **158**, 161104.
66 P. G. Bruce and C. A. Vincent, *J. Electroanal. Chem. Interfacial Electrochem.*, 1987, **225**, 1–17.
67 L. A. Woolf and K. R. Harris, *J. Chem. Soc., Faraday Trans. 1*, 1978, **74**, 933–947.
68 Y. Shao, H. Gudla, D. Brandell and C. Zhang, *J. Am. Chem. Soc.*, 2022, **144**, 7583–7587.
69 Y. Ma, M. Doyle, T. F. Fuller, M. M. Doeff, L. C. D. Jonghe and J. Newman, *J. Electrochem. Soc.*, 1995, **142**, 1859–1868.
70 A. Mistry, L. S. Grundy, D. M. Halat, J. Newman, N. P. Balsara and V. Srinivasan, *J. Electrochem. Soc.*, 2022, **169**, 040524.
71 M. Lorenz, F. Kilchert, P. Nürnberg, M. Schammer, A. Latz, B. Horstmann and M. Schönhoff, *J. Phys. Chem. Lett.*, 2022, **13**, 8761–8767.
72 Y. Zhou and G. H. Miller, *J. Phys. Chem.*, 1996, **100**, 5516–5524.
73 D. G. Miller, *J. Phys. Chem.*, 1986, **90**, 1509–1519.
74 J. G. Kirkwood, R. L. Baldwin, P. J. Dunlop, L. J. Gosting and G. Kegeles, *J. Chem. Phys.*, 1960, **33**, 1505–1513.
75 F. Kilchert, M. Lorenz, M. Schammer, P. Nürnberg, M. Schönhoff, A. Latz and B. Horstmann, *Phys. Chem. Chem. Phys.*, 2023, –.
76 S. de Groot and P. Mazur, *Non-equilibrium Thermodynamics*, North-Holland Publishing Company, 1962.
77 R. He and T. Kyu, *Macromolecules*, 2016, **49**, 5637–5648.
78 G. Orädd, L. Edman and A. Ferry, *Solid State Ionics*, 2002, **152-153**, 131–136.
79 B. K. Wheatle, N. A. Lynd and V. Ganesan, *ACS Macro Lett.*, 2018, **7**, 1149–1154.
80 K.-H. Shen and L. M. Hall, *Macromolecules*, 2020, **53**, 3655–3668.
81 K.-H. Shen and L. M. Hall, *Macromolecules*, 2020, **53**, 10086–10096.
82 H. Gudla, Y. Shao, S. Phunnarungsi, D. Brandell and C. Zhang, *J. Phys. Chem. Lett.*, 2021, **12**, 8460–8464.
83 N. M. Vargas-Barbosa and B. Roling, *ChemElectroChem*, 2020, **7**, 367–385.
84 P. Johansson, S. P. Gejji, J. Tegenfeldt and J. Lindgren, *Electrochimica Acta*, 1998, **43**, 1375–1379.
85 R. Arnaud, D. Benrabah and J.-Y. Sanchez, *J. Phys. Chem.*, 1996, **100**, 10882–10891.
86 P. Nürnberg, J. Atik, O. Borodin, M. Winter, E. Paillard and M. Schönhoff, *J. Am. Chem. Soc.*, 2022, **144**, 4657–4666.
87 A. Mistry, Z. Yu, B. L. Peters, C. Fang, R. Wang, L. A. Curtiss, N. P. Balsara, L. Cheng and V. Srinivasan, *ACS Central Sci.*, 2022, **8**, 880–890.
88 K. Ueno, K. Yoshida, M. Tsuchiya, N. Tachikawa, K. Dokko and M. Watanabe, *J. Phys. Chem. B*, 2012, **116**, 11323–11331.
89 D. Dong, F. Sälzer, B. Roling and D. Bedrov, *Phys. Chem. Chem. Phys.*, 2018, **20**, 29174–29183.
90 E. Ruckenstein and I. Shulgin, *Fluid Phase Equilibria*, 2001, **180**, 345–359.
91 I. Villaluenga, D. M. Pesko, K. Timachova, Z. Feng, J. Newman, V. Srinivasan and N. P. Balsara, *J. Electrochem. Soc.*, 2018, **165**, A2766–A2773.
92 R. Krishna and J. M. van Baten, *Ind. & Eng. Chem. Research*, 2005, **44**, 6939–6947.
93 L. Edman, *J. Phys. Chem. B*, 2000, **104**, 7254–7258.
94 I. Rey, J. Lassègues, J. Grondin and L. Servant, *Electrochimica Acta*, 1998, **43**, 1505–1510.
95 A. Bakker, J. Lindgren and K. Hermansson, *Polymer*, 1996, **37**, 1871–1878.
96 A. Stukowski, *Model. Simul. Mater. Sci. Eng.*, 2009, **18**, 015012.
97 C. Fang, W. S. Loo and R. Wang, *Macromolecules*, 2021, **54**, 2873–2881.
98 M. Rosso, T. Gobron, C. Brissot, J.-N. Chazalviel and S. Lascaud, *J. Power Sources*, 2001, **97-98**, 804–806.
99 A. G. Baboul, P. C. Redfern, A. Sutjianto and L. A. Curtiss, *J. Am. Chem. Soc.*, 1999, **121**, 7220–7227.
100 J. Mindemark, M. J. Lacey, T. Bowden and D. Brandell, *Prog. Polymer Sci.*, 2018, **81**, 114–143.
101 S. B. Aziz, T. J. Woo, M. Kadir and H. M. Ahmed, *J. Sci. Adv. Mater. Devices*, 2018, **3**, 1–17.
102 L. Long, S. Wang, M. Xiao and Y. Meng, *J. Mater. Chem. A*, 2016, **4**, 10038–10069.